

Article

Facile Preparation of Carbon Nitride-ZnO Hybrid Adsorbent for CO₂ Capture: The Significant Role of Amine Source to Metal Oxide Ratio

Siti Aishah Anuar, Khairul Naim Ahmad , Ahmed Al-Amiery , Mohd Shahbudin Masdar 
and Wan Nor Roslam Wan Isahak * 

Department of Chemical and Process Engineering, Faculty of Engineering and Built Environment, Universiti Kebangsaan Malaysia, Bangi 43600, Selangor, Malaysia; aishahofficial@yahoo.com (S.A.A.); khairulnaim021@gmail.com (K.N.A.); dr.ahmed1975@ukm.edu.my (A.A.-A.); shahbud@ukm.edu.my (M.S.M.)
* Correspondence: wannorroslam@ukm.edu.my; Tel.: +60-389216424

Abstract: The presence of CO₂ in gaseous fuel and feedstock stream of chemical reaction was always considered undesirable. High CO₂ content will decrease quality and heating value of gaseous fuel, such as biohydrogen, which needs a practical approach to remove it. Thus, this work aims to introduce the first C₃N₄-metal oxide hybrid for the CO₂ cleaning application from a mixture of CO₂-H₂ gas. The samples were tested for their chemical and physical properties, using field emission scanning electron microscopy (FESEM), transmission electron microscopy (TEM), physical adsorption analysis (BET), fourier-transform infrared (FTIR), x-ray diffraction (XRD), and x-ray photoelectron spectroscopy (XPS). The CO₂ capacity test was carried out by means of a breakthrough test at 1 atm and 25 °C using air as a desorption system. Among the samples, amine/metal oxide mass ratio of 2:1 (CNHP500-2(2-1)) showed the best performance of 26.9 wt. % (6.11 mmol/g), with a stable capacity over 6 consecutive cycles. The hybrid sample also showed 3 times better performance than the raw C₃N₄. In addition, it was observed that the hydrothermal C₃N₄ synthesis method demonstrated improved chemical properties and adsorption performance than the conventional dry pyrolysis method. In summary, the performance of hybrid samples depends on the different interactive factors of surface area, pore size and distribution, basicity, concentration of amine precursors, ratio of amines precursors to metal oxide, and framework stability.

Keywords: nitrogen-containing compounds; mesoporous structure; biohydrogen; physical adsorption; CO₂ capture



Citation: Anuar, S.A.; Ahmad, K.N.; Al-Amiery, A.; Masdar, M.S.; Wan Isahak, W.N.R. Facile Preparation of Carbon Nitride-ZnO Hybrid Adsorbent for CO₂ Capture: The Significant Role of Amine Source to Metal Oxide Ratio. *Catalysts* **2021**, *11*, 1253. <https://doi.org/10.3390/catal11101253>

Academic Editor: Edward G. Gillan

Received: 7 September 2021

Accepted: 16 October 2021

Published: 18 October 2021

Publisher's Note: MDPI stays neutral with regard to jurisdictional claims in published maps and institutional affiliations.



Copyright: © 2021 by the authors. Licensee MDPI, Basel, Switzerland. This article is an open access article distributed under the terms and conditions of the Creative Commons Attribution (CC BY) license (<https://creativecommons.org/licenses/by/4.0/>).

1. Introduction

Proton-exchange membrane fuel cell (PEMFC) technology is considered a promising energy source to meet the growing demand for energy supply [1]. Apart from the use of renewable fuel, its waste, which consists only of water, is environmentally friendly. However, it requires high-purity hydrogen gas fuel with more than 99.97% quality, as stated by the International Organization for Standardization (ISO FDIS14687-2) [2]. Traditional H₂ production from fossil fuels has been able to supply the desired fuels but with a persistent fossil depletion and release of carbon dioxide (CO₂) into the environment during its production process. As a result, biohydrogen gas was seen as a greener method of producing hydrogen (H₂). To date, raw biohydrogen gas typically consists of H₂-CO₂ mixture with a CO₂ ratio of 40–50 %. Therefore, the collected gas must first be purified by removing CO₂ by using either solid, liquid, or membrane adsorbents [3–5].

Scientists have attempted for years to absorb CO₂ using various solid adsorbents, such as activated carbon, silica, zeolite, and metal-organic frameworks [6–8]. Common improvement works are carried out by impregnation of amine additives, such as dimethylamine and polyethylamine (PEI), on their materials, assuming that the adsorbent basicity

thus increases the affinity of CO₂ gas to the adsorbent. However, issues, such as low CO₂ adsorption performance, low sample basicity, and sample degradation over repetitive cycles, are still under discussion. This study thus aims to use a material that is readily amine-rich, such as carbon nitride (C₃N₄), as an adsorbent support. C₃N₄ is a graphene-like organic material with an orderly 2D structure and a high nitrogen content. Apart from that, C₃N₄ possesses unique properties such as moderate band gap, nitrogen richness, and high thermal and chemical stability, making it a good photocatalyst, electrocatalyst, photoelectrocatalyst, as well as gas adsorbent for energy storage [9–12]. The materials can also be prepared by using low-cost precursors, such as urea, melamine, and dicyanamide [13].

To date, few studies have been performed to capture CO₂ on C₃N₄. However, they showed weak CO₂ adsorption performance due to their low porosity when they exist in bulk structures. Few researchers have tried to improve the performance of C₃N₄ by enhancing its porosity through a hard template method, apart from impregnating it with an amine-rich source, such as dimethylamine and PEI. However, the performance will eventually decrease due to PEI volatilization at temperatures above 100 °C and sample degradation over continuous cycles [14,15]. In some situations, a high-pressure operation may lead to favorable performance but with a high operating cost [16,17]. It is important to note that several preparation steps are needed for the common hard template process. Thus, preparing a C₃N₄ sample with a simpler route but still with a high yield and capturing performance is necessary.

On the other hand, few researchers have investigated the role of various metal oxides in the capture of CO₂, such as lithium oxide, calcium oxide, and magnesium oxide [18,19]. However, apart from the chemical sorption problems, these materials are costly. Zinc oxide is considered to be a favorable candidate for its low cost and easy regeneration of oxides. This is due to the formation of slightly exothermic and stable physisorption states between the CO₂ and polar ZnO surfaces by a linear adsorption mode [20]. In addition, small binding energies (0.06–0.1 eV) between zinc oxide and CO₂ indicate that the CO₂ adsorption and desorption process can easily occur instead of activating the reaction [20,21]. Past research also showed a positive effect of temperature and pressure on the CO₂ uptake of ZnO adsorbent [22]. To date, the hybridization of ZnO onto C₃N₄ has not been recorded for CO₂ capture studies. Hence, by a simple hydrothermal and pyrolysis process, we report the production of high-yield carbon nitride and zinc oxide hybrids. Firstly, we concentrated on raw C₃N₄ and C₃N₄-ZnO hybrid development via traditional dry-pyrolysis process. Then, we construct a more stable hybrid sample through the double preparation route with different ratio of amine to metal oxide. In short, we aim to manufacture a high-yield hybrid with high CO₂ capture performance.

2. Results and Discussion

Initial morphology test was performed by using field emission scanning electron microscopy (FESEM) analysis of sample CNHP500-2(2-1) as shown in Figure 1a,b. The hybrid sample displayed an exfoliated and agglomerated structure of C₃N₄ with a coral-reef-like framework. Sample measurement was recorded as 2 μm. In the meantime, detailed structure analysis through transmission electron microscopy (TEM) shows a dispersion of crystalline lattice clusters in a dimension of 10 nm (Figure 1c). These lattice structures with parallel array framework may indicate good hybridization of ZnO clusters on modified C₃N₄, as seen in Figure 1d.

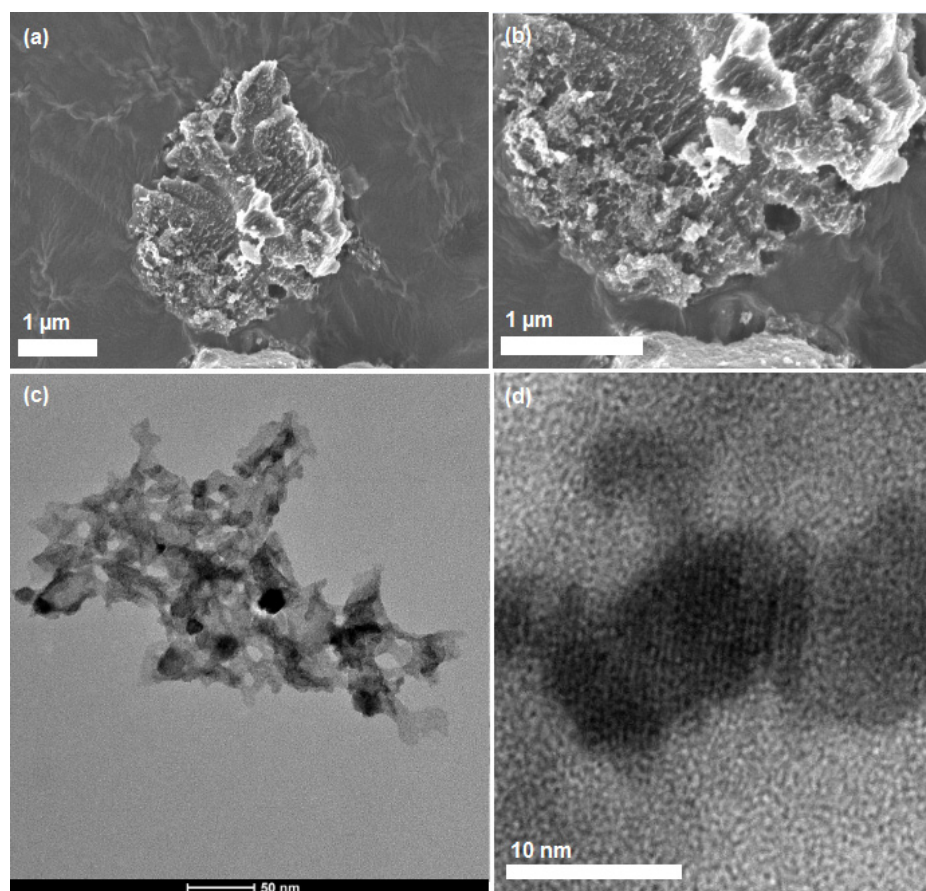


Figure 1. Field emission scanning electron microscopy (FESEM) micrographs of CNHP500-2(2-1) in (a) 5000 \times and (b) 10,000 \times magnifications. (c,d) TEM images of sample CNHP500-2(2-1).

Brunauer-Emmett-Teller (BET) technique was conducted to further assess the sample surface area and pore morphology. Figure 2 shows the nitrogen adsorption isotherm and their corresponding pore size distribution curves for sample CNHP500-2(4-1), CNHP500-2(3-1), and CNHP500-2(2-1). Sample CNHP500-2(3-1) displayed the highest surface area of 36.3 m²/g, with average pore diameter of 18.1 nm. Meanwhile, samples CNHP500-2(4-1) and CNHP500-2(2-1) displayed a surface area of 18.2 and 12.3 m²/g with pore size of 17.4 and 42.5 nm, respectively (Table 1). Although all samples displayed the same multilayer adsorption isotherm with mesoporous saturation point (Type V), each had different pore distribution curves. The pore numbers of sample CNHP500-2(4-1) is higher than sample CNHP500-2(3-1), with similar pore size uniformity. Meanwhile, sample CNHP500-2(2-1) displayed the lowest pore number counts and least uniform pore size distribution. In summary, the optimal amine to metal oxide ratio with the maximum surface area and uniform pore distribution is 3:1.

The samples were then characterized by using Fourier transformation infrared (FTIR) spectroscopy (Figure 3a). As shown by CN500 and CNH500 spectrum, the strong peak at 806 cm⁻¹ can be attributed to the triazine unit vibration of C₃N₄; the peak at 1240, 1327, 1412, and 1465 cm⁻¹ can be assigned to aromatic C–N heterocyclic stretching mode [23]; meanwhile, the peak at 1568 and 1635 cm⁻¹ represents the stretching mode of C–N and C=N [24]. The broad band between 3000–3674 cm⁻¹ can be correlated to the terminal amine group (–NH₂ or =NH) and hydroxyl (O–H) vibration [13]. For CNHP500-1, the spectrum resembles the CN500 band but in a weakened intensity, revealing overlapping bands of C₃N₄ and ZnO. Both CNHP500-1 and CNHP500-2(2-1) had a weak peak around 2200 cm⁻¹, suggesting that modification with zinc acetate at 2:1 ratio promotes nitrile bond C≡N formation, as detailed by Deng and co-workers [14]. Since CNHP500-2 preparation

was modified through a hydrothermal synthesis, the typical spectrum of C_3N_4 was again reserved as seen in Figure 3b. This was due to the universal solvent properties of water that dissolve all polar reactants during preparation steps. All CNHP500-2(4-1), CNHP500-2(3-1), and CNHP500-2(2-1) samples exhibited the same functional group properties, with peak intensity decreases in the order of decreasing amine to metal oxide ratio. It may also be noted that an amine to metal oxide ratio higher than 2:1 does not promote nitrile formation.

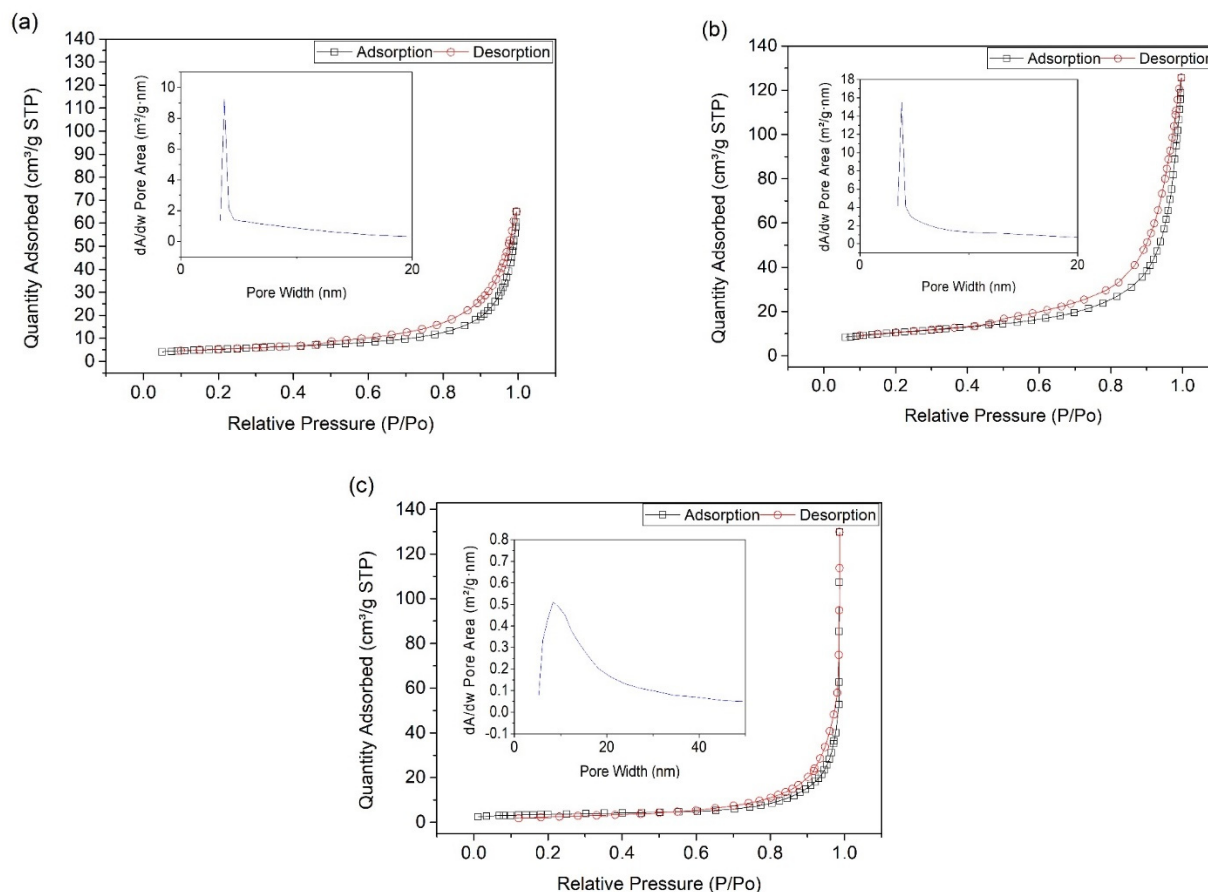


Figure 2. Nitrogen adsorption-desorption isotherms and their corresponding pore size distribution curves (inset) for sample (a) CNHP500-2(4-1), (b) CNHP500-2(3-1), and (c) CNHP500-2(2-1).

Table 1. Textural properties of the adsorbents.

Sample	BET Surface Area (m^2/g)	Pore Size (nm)
CNHP500-2(2-1)	12.3	42.5
CNHP500-2(3-1)	36.3	18.1
CNHP500-2(4-1)	18.2	17.4

Powder X-ray diffraction (XRD) analysis was done to study the sample crystalline properties (Figure 4). The XRD patterns of sample CN500, CNH500, CNHP500-2(4-1), CNHP500-2(3-1), and CNHP500-2(2-1) showed a sharp peak at 27.4° , 27.2° , 27.7° , 27.7° , and 27.2° , respectively. It can be assigned as the turbo static ordering of carbon and nitrogen atoms (002) in CN-graphene like layers with a uniform distribution of N atoms. While Niu and co-workers suggested a reduction of gallery distance when a peak shift towards higher angle, a shift to the lower angle suggests an improvement in the gallery distance between the basic sheets of $g-C_3N_4$ nanosheets due to ZnO incorporation, as shown by sample CNH500 and CNHP500-2(2-1) [25]. A slightly broad peak of CNHP500-2(2-1) suggested a semi-crystalline nature that can be related to the fabrication of amorphous carbon in the

sample. For CNHP500-1, a wide and diffusing peak indicate an assembly of a randomly arranged amorphous structure. This can be ascribed to the incorporation of metal oxide caused the interference of crystal growth of C_3N_4 [26]. Meanwhile, an additional peak at 13.3° of all samples indicates the in-plane structural packing motif indexed as (100) phase of $g-C_3N_4$ [27]. Additionally, the low-intensity diffraction peaks related to ZnO were detected at 32° , 34° , and 36° . However, the peaks were not visible in sample CNHP500-2(3-1), suggesting smaller crystallite size or highly dispersed of ZnO particles on the C_3N_4 mesoporous surface.

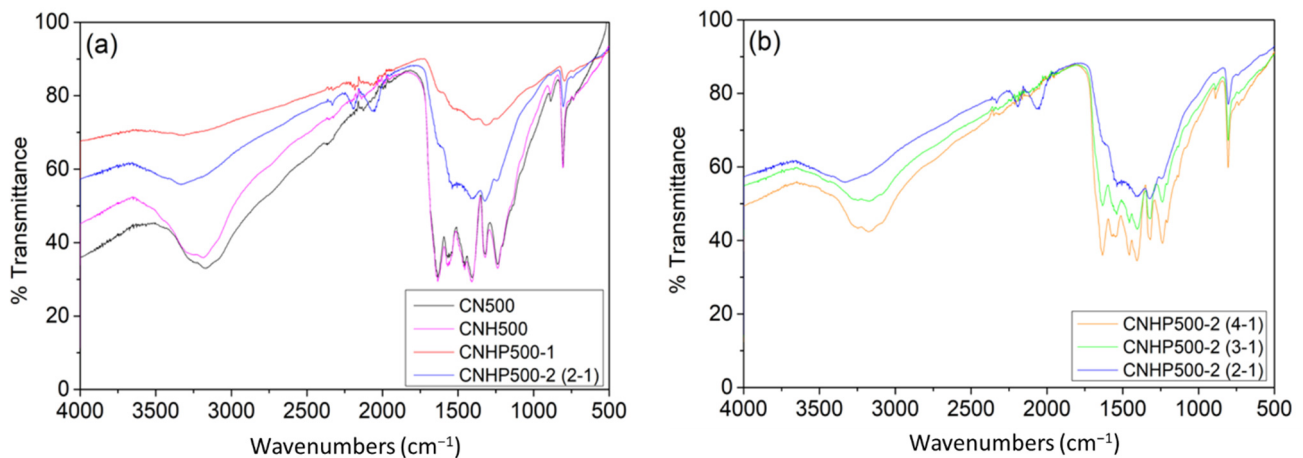


Figure 3. (a) FTIR spectra for sample CN500, CNH500, CNHP500-1, and CNHP500-2(2-1). (b) FTIR spectra for sample CNHP500-2(4-1), CNHP500-2(3-1), and CNHP500-2(2-1).

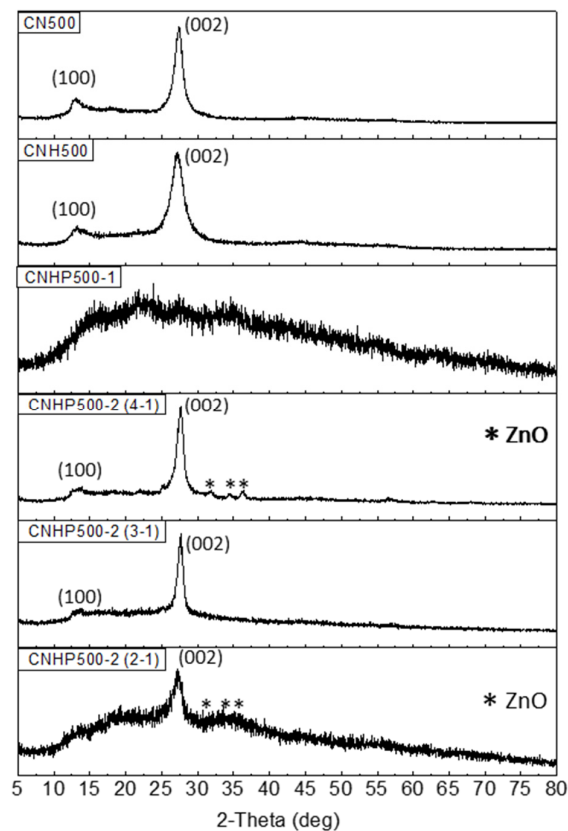


Figure 4. X-ray diffraction (XRD) patterns for the sample CN500, CNH500, CNHP500-1, CNHP500-2(4-1), CNHP500-2(3-1), and CNHP500-2(2-1).

The X-ray photoelectron spectroscopy (XPS) analysis was further carried out to analyse the elemental composition of sample. From Figure 5, it can be seen that both CN500 and CNH500 displayed a typical spectrum of carbon nitride, with peaks of C 1s and N 1s at 285 and 396 eV, respectively. Meanwhile, the survey spectra of CNHP500-1 and CNHP500-2(2-1) showed obvious signals from elements C, N, O, and Zn, indicating the successful formation of C_3N_4 -ZnO hybrid. It proves that the second synthesis method is better than the first method given the differences in intensity. The C 1s deconvolution spectrum of CNHP500-2(2-1) represents the C-C and C-N interaction at the binding energy of 284.5 and 288.2 eV [28]. Meanwhile, the peak of O 1s at 529.7 eV signifies the Zn-O interaction [29]. For N 1s, the peak at 397 eV indicates the formation of pyridinic-N structure [13] as the best basic site for CO_2 interaction. The pyridinic-N is considered the most favorable site for CO_2 binding owing to its high Lewis basic characteristic [30]. The formation of Zn^{2+} , with peaks at 1021.7 and 1044.7 eV, denotes the peak of Zn $2p_{3/2}$ and Zn $2p_{1/2}$ [31]. The elemental composition of CNHP500-2(2-1) sample (Table 2) revealed the atomic percentage of carbon, nitrogen, oxygen, zinc are 41.8, 22.3, 22.7, and 13.2%, respectively. This indicates that the content of C_3N_4 and ZnO in the sample are 64.1% and 35.9%, which is close to theoretical ratio of $C_3N_4:ZnO$ (2:1 or 66.7:33.3) in the CNHP500-2(2-1) sample.

Table 2. Surface elemental composition of CNHP500-2(2-1) sample.

Element	Atomic Percentage (at %)
C	41.8
N	22.3
O	22.7
Zn	13.2

For the final analysis, the adsorbent samples were further tested for CO_2 adsorption-desorption activity at low temperature and pressure. Figure 6 represents the adsorption curves (a), desorption curves (b), and CO_2 capture capacity (c) for all samples. In the meantime, Figure 6d represents the adsorption capacity of sample CNHP500-2(4-1), CNHP500-2(3-1), and CNHP500-2(2-1) for three consecutive cycles. Based on adsorption and desorption curves, the samples CNHP500-2(3-1) and CNHP500-2(4-1) exhibited a longer time for CO_2 adsorption compared to other samples, but steeper curves of desorption were shown, suggesting a more complex and time-consuming desorption process. On the other hand, CNHP500-2(2-1) and CNHP500-1 samples demonstrated a rapid and easy desorption of CO_2 , which is beneficial for efficient adsorption cycle.

In terms of capture performance, sample CNHP500-2(2-1) displayed the highest adsorption capacity of 26.9 wt. %. The sample displayed 3-fold higher CO_2 adsorption capacity when compared to CNHP500-1, although both samples were prepared with similar amine to metal oxide ratio. This shows the importance of water as a universal solvent during hydrothermal synthesis in contrast to the conventional dry-pyrolysis method. Meanwhile, the performance of hybrid samples with different amine to metal oxide ratio displayed an increasing adsorption capacity in the order of CNHP500-2(4-1) < CNHP500-2(3-1) < CNHP500-2(2-1). This can be attributed to the increasing numbers of metal oxide per active site in the sample. Theoretically, C_3N_4 linkages are good for CO_2 capture because they provide the required basic site for acidic CO_2 adsorption activities. Recent analysis of density functional theory (DFT) between CO_2 and C_3N_4 materials shows that the weak van der Waals bond form by abundantly accessible pyridinic-N structure of C_3N_4 has been favorable for CO_2 interaction [32]. On the other hand, metal oxide ZnO can further enhance the intensity of accessible active site by forming low binding strength interaction, as explained by Tang and co-workers [20]. That explained why the hybrid samples performed better than a pure C_3N_4 (CN500). As for the three-cycle adsorption test in Figure 6d, CNHP500-2(2-1) sample showed a decrease in capture capacity after the first to second cycles and then slight increase towards the third cycle. Furthermore, CHNP500-2(3-1) sample also demonstrated similar performance in the second and third

cycles. However, considering the desorption isotherms in Figure 6b, CNHP500-2(2-1) sample demonstrated far more rapid and easier desorption process for CO₂ compared to CNHP500-2(3-1), suggesting better adsorbent characteristics. Further raising the ratio to 4:1 would not be advantageous for the capture performance, as the low CO₂ capture capacities of CNHP500-2(4-1) sample were shown in all three consecutive cycles. This can be explained by the reduced amount of ZnO on the adsorbent surface as the ratio increases, thus lessening the promotional effects of ZnO.

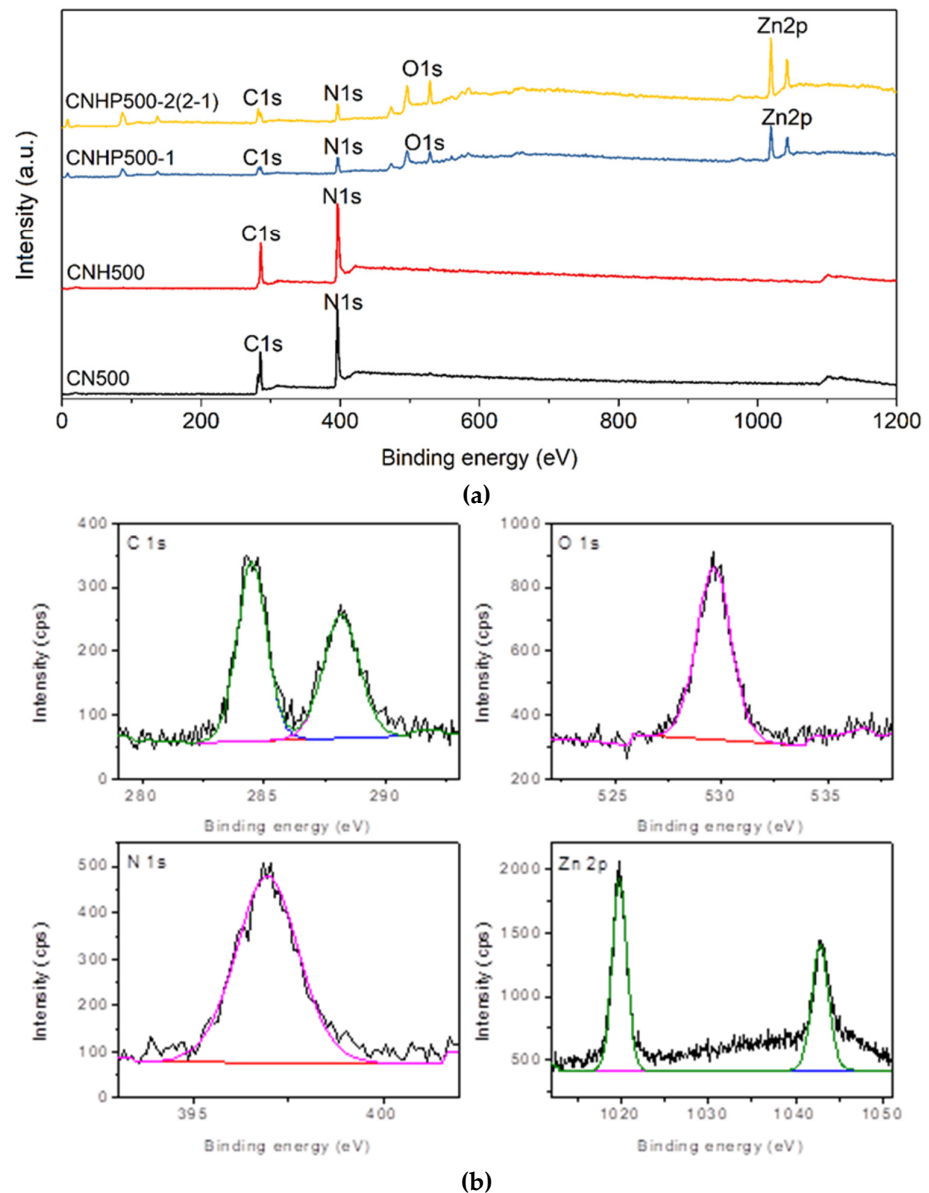


Figure 5. (a) Wide x-ray photoelectron spectroscopy (XPS) spectra for sample CN500, CNH500, CNHP500-1, and CNHP500-2(2-1) and (b) the corresponding Gaussian–Lorentzian deconvolution shapes for C1s, O1s, N1s, and Zn 2p of sample CNHP500-2(2-1).

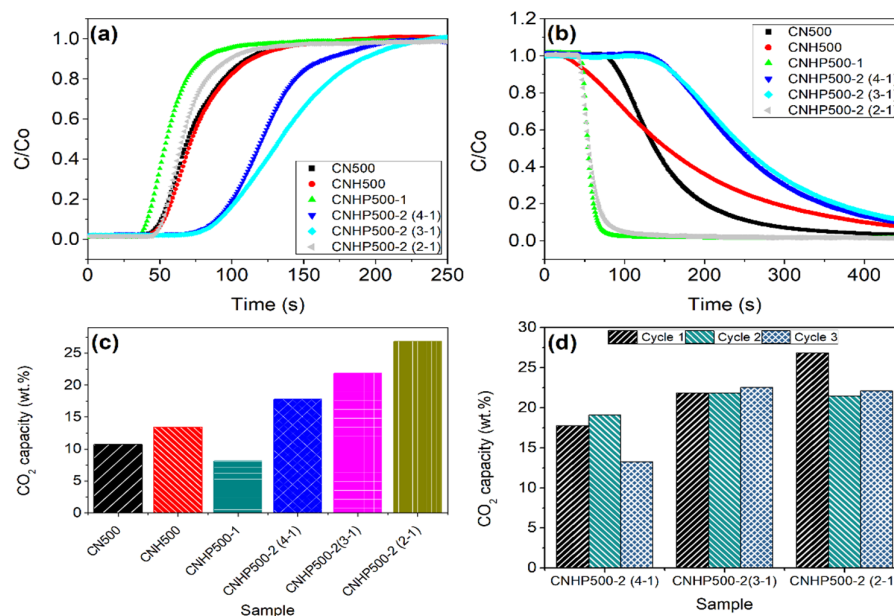


Figure 6. (a) Adsorption and (b) desorption isotherm of sample CN500, CNH500, CNHP500-1, CNHP500-2(4-1), CNHP500-2(3-1), and CNHP500-2(2-1). (c) CO₂ capture capacity of different samples at 50 ml/min and room condition (1 atm, 25 °C). (d) CO₂ capture capacity of sample CNHP500-2(4-1), CNHP500-2(3-1), and CNHP500-2(2-1) for 3 continuous cycles.

The effect of melamine and urea combination in C₃N₄ synthesis can be seen in sample CNH500. Compared to a pure melamine-based C₃N₄ (CN500), the sample displayed a better adsorption capacity, as in Figure 6c. Similar to a study by Zheng and co-workers, the incorporation of urea created a disturbance during C₃N₄ formation, thus providing a higher sheet gap and a better surface area [33–36]. To note, all hybrid samples in this study applied the combination of melamine and urea as the amine source to boost the sheet gap and surface contact area.

To further comprehend the stability of the best sample, CNHP500-2(2-1) was tested for adsorption-desorption activity over six continuous cycles. Based on Figure 7a, the sample showed a rapid overall cycle with a complete cycle measured as 20 minutes each, indicating a quick adsorption-desorption process. Figure 7b displayed a sharp and consistent adsorption isotherm of sample except at the first cycle. In terms of desorption activity, the result from Figure 7c clearly showed an excellent profile consistency for over six cycles. Hence, fast desorption activity confirms the absence of major clogging issue. Based on Figure 7d, the sample displayed high and consistent CO₂ adsorption capacity, which indicated a low material degradation rate. Meanwhile, a slight decline in CO₂ capacity for the second cycle afterwards can be explained by several factors, such as the pore heterogeneity or arrangement and minor chemical adsorption. In terms of moisture consequence on CO₂ capture performance, the durability of the sample was proven through the usage of air as desorbing gas. Although there is a little percentage of moisture in the air, the sample still displayed a stable CO₂ capacity.

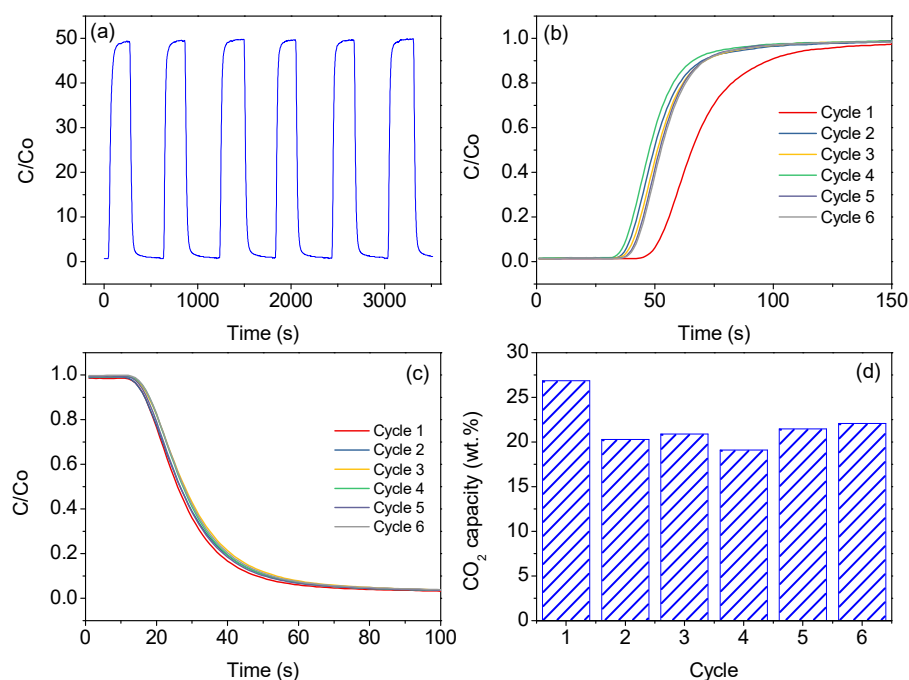


Figure 7. (a) Continuous CO₂ capture profile, (b) adsorption isotherm, (c) desorption isotherm, and (d) CO₂ capture capacity of sample CNHP500-2(2-1) for 6 consecutive cycles at 50 ml/min and room condition (1 atm, 25 °C).

3. Materials and Methods

3.1. Chemical and Reagents

Reagent grade melamine powder was purchased from Sigma-Aldrich, Saint Louis, MO, USA. Meanwhile, urea and zinc acetate powder were purchased from R&M Chemicals (London, UK). CO₂-H₂ gas mixture with vol. % of 50:50 was supplied by Linde Malaysia Sdn Bhd, Selangor, Malaysia. All materials were used without further treatment.

3.2. Synthesis of Adsorbents

A carbon nitride hybrid with porogen sample, namely CNHP500-1, was prepared via a simple dry in-situ pyrolysis method (1st method). Initially, amine sources (urea and melamine) and zinc acetate were placed into a closed-lid crucible and underwent pyrolysis at 500 °C for 1 h. The sample was left to cool at room temperature for 24 h before being ground into fine powder in a mortar. Meanwhile, the sample hybrid CNHP500-2(x-y), where x-y represent the amine to metal oxide mass ratio, was prepared through a facile hydrothermal and pyrolysis method (2nd method). Initially, appropriate amounts of the amine sources (urea and melamine) and zinc acetate were added with water and stirred for 24 h. The resulting solution was sonicated and dried for 24 h. The dried sample was then pyrolyzed at 500 °C for 1 h under closed crucible. The sample was left to cool for 24 h before being ground into powder. The ratios of amine to metal oxide of 2:1, 3:1, and 4:1 were denoted as CNHP500-2(2-1), CNHP500-2(3-1), and CNHP500-2(4-1), respectively. For comparison, bulk C₃N₄ namely CN500 was prepared through the conventional dry-pyrolysis of melamine powder at 500 °C for 1 h. Another bulk C₃N₄ sample was prepared through direct pyrolysis of melamine-urea mixture in 1:1 mass ratio at 500 °C for 1 h and was labelled as CNH500. Table 3 summarizes the samples synthesized in this study.

Table 3. Summary of the samples prepared in the study.

Sample	Method	Amine Source	Amine/Metal Oxide Mass Ratio
CN500	Dry pyrolysis	Melamine	-
CNH500	Dry pyrolysis	Melamine and urea	-
CNHP500-1	Dry pyrolysis	Melamine and urea	2:1
CNHP500-2(2-1)	Hydrothermal and dry pyrolysis	Melamine and urea	2:1
CNHP500-2(3-1)	Hydrothermal and dry pyrolysis	Melamine and urea	3:1
CNHP500-2(4-1)	Hydrothermal and dry pyrolysis	Melamine and urea	4:1

3.3. Characterization

To view the sample morphology, field emission scanning electron microscopy (FESEM) and transmission electron microscopy (TEM) was carried out using SEM ZEISS Supra 55 VP (Oberkochen, Germany) and TEM Thermo Fischer (Model Talos 120C) (OR, USA), respectively. Textural analysis was conducted using Micromeritics ASAP 2020 (Norcross, GA, USA) with Brunauer–Emmett–Teller (BET) model was used to determine the specific surface area. Bulk Scientific M, Perkin Elmer (Waltham, MA, USA) Fourier-transform infrared (FTIR) spectrophotometer was used to analyze the functional groups. FTIR ATR sampling technique was applied while the sample used, as it is in powder form. Sample crystallinity study was conducted via X-ray diffraction (XRD) by Bruker AXS D8 Advance diffractometer (Bremen, Germany) operating at 40 kV and 40 mA using Ni filtered Cu K α source ($\lambda = 0.15406$ nm), and XRD patterns were measured between $2\theta = 5 - 80^\circ$ at a scan rate $0.25^\circ \text{ s}^{-1}$. Meanwhile, X-ray photoelectron spectroscopy (XPS) analysis was employed on Kratos/Shimadzu Axis Ultra DLD (Manchester, UK), with Al K α (1486 eV) monochromatic X-ray as the excitation source.

3.4. CO₂ Capture Test

The CO₂ capture test was done through a breakthrough experiment, as in previous study [37]. In summary, the sample was packed into a column before being connected to gas-flowmeter-sample-CO₂ analyzer system. A CO₂ analyzer from Quantek Instrument Model 906 (Grafton, MA, USA) was used with HOBOWare software (HOBOWare Pro 3.7.18 version, Onset, Cape Cod, Massachusetts, USA, 2018) as data logger. All tests were conducted on a fixed flowrate of 50 mL/min at room temperature and pressure.

4. Conclusions

To conclude, the C₃N₄-ZnO organic-inorganic hybrid, namely CNHP500-2(2-1), was successfully prepared via a facile hydrothermal and pyrolysis route. The simplistic fabrication of this sample, with low cost with high yield, high CO₂ capture capacity, and high sample stability, qualify it as a prospective adsorbent for future CO₂ removal application. To highlight, past C₃N₄ studies for CO₂ capture application favored a high surface area sample via hard template synthesis to improve the mass transport of gas. Through this study, a low surface area C₃N₄ with optimal ratio of metal oxide hybridisation, a disturbed sheet of N heterogens, and favorable bond strength between adsorbent and adsorbate was able to display a comparable CO₂ capture performance. Thus, the synthesis of abundantly graphitic-N C₃N₄ with ZnO hybridization is an interesting and promising study that may be conducted in the near future. Above all, we hope this work can open a new path to the development of a versatile adsorbent for CO₂ capture soon.

Author Contributions: Conceptualization, S.A.A. and W.N.R.W.I.; methodology, S.A.A. and W.N.R.W.I.; validation, A.A.-A., M.S.M. and W.N.R.W.I.; formal analysis, S.A.A., K.N.A. and A.A.-A. Investigation S.A.A.; resources, S.A.A. and W.N.R.W.I.; data curation, S.A.A. and W.N.R.W.I.; writing—original draft preparation, S.A.A.; writing—review and editing, K.N.A., A.A.-A., M.S.M. and W.N.R.W.I.; visualization, S.A.A. and W.N.R.W.I.; supervision, M.S.M. and W.N.R.W.I.; project administration, W.N.R.W.I.; funding acquisition, W.N.R.W.I. All authors have read and agreed to the published version of the manuscript.

Funding: This research was funded by the Ministry of Higher Education of Malaysia under research code FRGS/1/2020/TK0/UKM/02/31 and Universiti Kebangsaan Malaysia under research code GUP-2020-012 and GP-2020-K020823.

Data Availability Statement: All relevant data are contained in the present manuscript. Other inherent data are available on request from the corresponding author.

Acknowledgments: This research was supported by the Ministry of Higher Education of Malaysia under research code Fundamental Research Grant Scheme (FRGS/1/2020/TK0/UKM/02/31) and Universiti Kebangsaan Malaysia under research code GUP-2020-012 and GP-2020-K020823.

Conflicts of Interest: The authors declare no conflict of interest.

References

1. Sun, X.; Xu, K.; Fleischer, C.; Liu, X.; Grandcolas, M.; Strandbakke, R.; Bjørheim, T.S.; Norby, T.; Chatzitakis, A. Earth-abundant electrocatalysts in proton exchange membrane electrolyzers. *Catalysts* **2018**, *8*, 657. [\[CrossRef\]](#)
2. Ohi, J.M.; Vanderborgh, N.; Voecks, G. *Hydrogen Fuel Quality Specifications for Polymer Electrolyte Fuel Cells in Road Vehicles: Report to the Safety, Codes and Standards Program*; US Department of Energy: Washington, DC, USA, 2016.
3. Ravi, N.; Anuar, S.A.; Yusuf, N.Y.M.; Isahak, W.N.R.W.; Masdar, M.S. Amine-mixed oxide hybrid materials for carbon dioxide adsorption from CO₂/H₂ mixture. *Mater. Res. Express* **2018**, *5*, 55501. [\[CrossRef\]](#)
4. Yusuf, N.Y.; Masdar, M.S.; Isahak, W.N.R.W.; Nordin, D.; Husaini, T.; Majlan, E.H.; Rejab, S.A.M.; Chew, C.L. Ionic liquid-impregnated activated carbon for biohydrogen purification in an adsorption unit. *IOP Conf. Ser. Mater. Sci. Eng.* **2017**, *206*, 12071. [\[CrossRef\]](#)
5. Wu, S.-Y.; Hsiao, I.-C.; Liu, C.-M.; Mt Yusuf, N.Y.; Wan Isahak, W.N.R.; Masdar, M.S. A novel bio-cellulose membrane and modified adsorption approach in CO₂/H₂ separation technique for PEM fuel cell applications. *Int. J. Hydrogen Energy* **2017**, *42*, 27630–27640. [\[CrossRef\]](#)
6. Sanz, R.; Calleja, G.; Arencibia, A.; Sanz-Pérez, E.S. Amino functionalized mesostructured SBA-15 silica for CO₂ capture: Exploring the relation between the adsorption capacity and the distribution of amino groups by TEM. *Microporous Mesoporous Mater.* **2012**, *158*, 309–317. [\[CrossRef\]](#)
7. Zhou, S.; Zou, X.; Sun, F.; Ren, H.; Liu, J.; Zhang, F.; Zhao, N.; Zhu, G. Development of hydrogen-selective CAU-1 MOF membranes for hydrogen purification by ‘dual-metal-source’ approach. *Int. J. Hydrogen Energy* **2013**, *38*, 5338–5347. [\[CrossRef\]](#)
8. Gil, M.V.; Álvarez-Gutiérrez, N.; Martínez, M.; Rubiera, F.; Pevida, C.; Morán, A. Carbon adsorbents for CO₂ capture from bio-hydrogen and biogas streams: Breakthrough adsorption study. *Chem. Eng. J.* **2015**, *269*, 148–158. [\[CrossRef\]](#)
9. Wen, J.; Xie, J.; Chen, X.; Li, X. A review on g-C₃N₄-based photocatalysts. *Appl. Surf. Sci.* **2017**, *391*, 72–123. [\[CrossRef\]](#)
10. Zheng, Y.; Jiao, Y.; Chen, J.; Liu, J.; Liang, J.; Du, A.; Zhang, W.; Zhu, Z.; Smith, S.C.; Jaroniec, M.; et al. Nanoporous Graphitic-C₃N₄@Carbon Metal-Free Electrocatalysts for Highly Efficient Oxygen Reduction. *J. Am. Chem. Soc.* **2011**, *133*, 20116–20119. [\[CrossRef\]](#)
11. Safaei, J.; Ullah, H.; Mohamed, N.A.; Mohamad Noh, M.F.; Soh, M.F.; Tahir, A.A.; Ahmad Ludin, N.; Ibrahim, M.A.; Wan Isahak, W.N.R.; Mat Teridi, M.A. Enhanced photoelectrochemical performance of Z-scheme g-C₃N₄/BiVO₄ photocatalyst. *Appl. Catal. B Environ.* **2018**, *234*, 296–310. [\[CrossRef\]](#)
12. Ansari, S.A.; Cho, M.H. Simple and Large Scale Construction of MoS₂-g-C₃N₄ Heterostructures Using Mechanochemistry for High Performance Electrochemical Supercapacitor and Visible Light Photocatalytic Applications. *Sci. Rep.* **2017**, *7*, 43055. [\[CrossRef\]](#)
13. Martha, S.; Nashim, A.; Parida, K.M. Facile synthesis of highly active g-C₃N₄ for efficient hydrogen production under visible light. *J. Mater. Chem. A* **2013**, *1*, 7816–7824. [\[CrossRef\]](#)
14. Deng, Q.-F.; Liu, L.; Lin, X.-Z.; Du, G.; Liu, Y.; Yuan, Z.-Y. Synthesis and CO₂ capture properties of mesoporous carbon nitride materials. *Chem. Eng. J.* **2012**, *203*, 63–70. [\[CrossRef\]](#)
15. Li, Q.; Yang, J.; Feng, D.; Wu, Z.; Wu, Q.; Park, S.S.; Ha, C.-S.; Zhao, D. Facile synthesis of porous carbon nitride spheres with hierarchical three-dimensional mesostructures for CO₂ capture. *Nano Res.* **2010**, *3*, 632–642. [\[CrossRef\]](#)
16. Lakhi, K.S.; Baskar, A.V.; Zaidi, J.S.M.; Al-Deyab, S.S.; El-Newehy, M.; Choy, J.-H.; Vinu, A. Morphological control of mesoporous CN based hybrid materials and their excellent CO₂ adsorption capacity. *RSC Adv.* **2015**, *5*, 40183–40192. [\[CrossRef\]](#)
17. Lakhi, K.S.; Park, D.-H.; Singh, G.; Talapaneni, S.N.; Ravon, U.; Al-Bahily, K.; Vinu, A. Energy efficient synthesis of highly ordered mesoporous carbon nitrides with uniform rods and their superior CO₂ adsorption capacity. *J. Mater. Chem. A* **2017**, *5*, 16220–16230. [\[CrossRef\]](#)
18. Zhang, Y.; Gao, Y.; Pfeiffer, H.; Louis, B.; Sun, L.; O’Hare, D.; Wang, Q. Recent advances in lithium containing ceramic based sorbents for high-temperature CO₂ capture. *J. Mater. Chem. A* **2019**, *7*, 7962–8005. [\[CrossRef\]](#)
19. Gunathilake, C.; Jaroniec, M. Mesoporous calcium oxide-silica and magnesium oxide-silica composites for CO₂ capture at ambient and elevated temperatures. *J. Mater. Chem. A* **2016**, *4*, 10914–10924. [\[CrossRef\]](#)
20. Tang, Q.-L.; Luo, Q.-H. Adsorption of CO₂ at ZnO: A Surface Structure Effect from DFT+U Calculations. *J. Phys. Chem. C* **2013**, *117*, 22954–22966. [\[CrossRef\]](#)

21. Farias, S.A.S.; Longo, E.; Gargano, R.; Martins, J.B.L. CO₂ adsorption on polar surfaces of ZnO. *J. Mol. Model.* **2013**, *19*, 2069–2078. [[CrossRef](#)]
22. Kumar, S. The effect of elevated pressure, temperature and particles morphology on the carbon dioxide capture using zinc oxide. *J. CO₂ Util.* **2014**, *8*, 60–66. [[CrossRef](#)]
23. Shcherban, N.D.; Mäki-Arvela, P.; Aho, A.; Sergiienko, S.A.; Yaremov, P.S.; Eränen, K.; Murzin, D.Y. Melamine-derived graphitic carbon nitride as a new effective metal-free catalyst for Knoevenagel condensation of benzaldehyde with ethylcyanoacetate. *Catal. Sci. Technol.* **2018**, *8*, 2928–2937. [[CrossRef](#)]
24. Wan, S.; Zhong, Q.; Ou, M.; Zhang, S. Highly efficient simulated solar-light photocatalytic oxidation of gaseous NO with porous carbon nitride from copolymerization with thymine and mechanistic analysis. *RSC Adv.* **2016**, *6*, 101208–101215. [[CrossRef](#)]
25. Niu, P.; Zhang, L.; Liu, G.; Cheng, H.-M. Graphene-Like Carbon Nitride Nanosheets for Improved Photocatalytic Activities. *Adv. Funct. Mater.* **2012**, *22*, 4763–4770. [[CrossRef](#)]
26. Ahmad, K.N.; Wan Isahak, W.N.R.; Rosli, M.I.; Yusop, M.R.; Kassim, M.B.; Yarmo, M.A. Rare earth metal doped nickel catalysts supported on exfoliated graphitic carbon nitride for highly selective CO and CO₂ methanation. *Appl. Surf. Sci.* **2022**, *571*, 151321. [[CrossRef](#)]
27. Fina, F.; Callear, S.K.; Carins, G.M.; Irvine, J.T.S. Structural Investigation of Graphitic Carbon Nitride via XRD and Neutron Diffraction. *Chem. Mater.* **2015**, *27*, 2612–2618. [[CrossRef](#)]
28. Alman, V.; Singh, K.; Bhat, T.; Sheikh, A.; Gokhale, S. Sunlight Assisted improved photocatalytic degradation of rhodamine B using Pd-loaded g-C₃N₄/WO₃ nanocomposite. *Appl. Phys. A* **2020**, *126*, 724. [[CrossRef](#)]
29. Nayak, P.K.; Wang, Z.; Anjum, D.H.; Hedhili, M.N.; Alshareef, H.N. Highly stable thin film transistors using multilayer channel structure. *Appl. Phys. Lett.* **2015**, *106*, 103505. [[CrossRef](#)]
30. Li, L.; Wang, Y.; Gu, X.; Yang, Q.; Zhao, X. Increasing the CO₂/N₂ Selectivity with a Higher Surface Density of Pyridinic Lewis Basic Sites in Porous Carbon Derived from a Pyridyl-Ligand-Based Metal–Organic Framework. *Chem. An Asian J.* **2016**, *11*, 1913–1920. [[CrossRef](#)]
31. Liang, Y.-C.; Wang, C.-C. Surface crystal feature-dependent photoactivity of ZnO–ZnS composite rods via hydrothermal sulfidation. *RSC Adv.* **2018**, *8*, 5063–5070. [[CrossRef](#)]
32. Wang, M.; Fan, X.; Zhang, L.; Liu, J.; Wang, B.; Cheng, R.; Li, M.; Tian, J.; Shi, J. Probing the role of O-containing groups in CO₂ adsorption of N-doped porous activated carbon. *Nanoscale* **2017**, *9*, 17593–17600. [[CrossRef](#)]
33. Zheng, Y.; Zhang, Z.; Li, C. A comparison of graphitic carbon nitrides synthesized from different precursors through pyrolysis. *J. Photochem. Photobiol. A Chem.* **2017**, *332*, 32–44. [[CrossRef](#)]
34. Huang, C.; Wen, Y.; Ma, J.; Dong, D.; Shen, Y.; Liu, S.; Ma, H.; Zhang, Y. Unraveling fundamental active units in carbon nitride for photocatalytic oxidation reactions. *Nat. Commun.* **2021**, *12*, 320. [[CrossRef](#)]
35. Ma, D.; Li, X.; Wang, X.; Luo, Y. Research development on graphitic carbon nitride and enhanced catalytic activity on ammonium perchlorate. *RSC Adv.* **2021**, *11*, 5729–5740. [[CrossRef](#)]
36. Ani, I.J.; Akpan, U.G.; Olutoye, M.A.; Hameed, B.H. Solar light responsive TiO₂-ZnO, modified with graphitic carbon nitride nano-sheet for degradation of AB29. *J. Chem. Technol. Biotechnol.* **2020**, *95*, 2674–2683. [[CrossRef](#)]
37. Anuar, S.A.; Wan Isahak, W.N.R.; Masdar, M.S. Carbon nanoflake hybrid for biohydrogen CO₂ capture: Breakthrough adsorption test. *Int. J. Energy Res.* **2020**, *44*, 3148–3159. [[CrossRef](#)]